This article has been accepted for publication in a future issue of this journal, but has not been fully edited. Content may change prior to final publication. Citation information: DOI 10.1109/TNB.2018.2870331, IEEE Transactions on NanoBioscience

Cardiac conduction model for generating 12 lead ECG signals with realistic heart rate dynamics

Mario A. Quiroz-Juárez, Omar Jiménez-Ramírez, Rubén Vázquez-Medina, Elena Ryzhii, Maxim Ryzhii, *Senior Member, IEEE*, and José L. Aragón*

***Abstract*—We present extended heterogeneous oscillator model of cardiac conduction system for generation of realistic 12 lead ECG waveforms. The model consists of main natural pacemakers represented by modified van der Pol equations, and atrial and ventricular muscles, in which the depolarization and repolarization processes are described by modified FitzHugh-Nagumo equations. We incorporate an artificial RR-tachogram with the specific statistics of a heart rate, the frequency-domain characteristics of heart rate variability produced by Mayer and respiratory sinus arrhythmia waves, normally distributed additive noise and a baseline wander that couple the respiratory frequency. The standard 12 lead ECG is calculated by means of a weighted linear combination of atria and ventricle signals and thus can be fitted to clinical ECG of real subject. The model is capable to simulate accurately realistic ECG characteristics including local pathological phenomena accounting for biophysical properties of the human heart. All these features provide significant advantages over existing nonlinear cardiac models. The proposed model constitutes a useful tool for medical education and for assessment and testing of ECG signal processing software and hardware systems.**

***Index Terms*—Heart model, 12 lead ECG, heart rate variability, cardiac conduction system, differential equations.**

I. Introduction

The ECG reflects the recorded potential difference between two electrodes placed on the surface of the skin. The largest amplitude of a single cycle of the normal ECG exposes the depolarization process of the ventricle and is referred to as the R-wave. The RR-interval is the time between successive R-peaks; a series of RR-intervals is known as RR-tachogram and the variability of this series reveals important information about the physiological state of the subject [1]. The instantaneous heart rate is given by the reciprocal of the RR-interval in beats per minute and it may be increased or decreased by sympathetic and parasympathetic, subsystems of the autonomic nervous system. The balance between the effects of the sympathetic and parasympathetic activity is referred to as the sympathovagal balance, and it is believed to be manifested in the beat-to-beat changes of the cardiac cycle [2].

The effect of the sympathetic and parasympathetic modulation on heart rate can be estimated from the spectral analysis of the heart rate variability (HRV), and this information can help to predict the state of the autonomic nervous system [3]. The two main frequency bands of interest in the power spectral of the HRV are referred to as the low frequency (LF) band (0.04-0.15 Hz) and the high frequency (HF) band (0.15-0.4 Hz). The LF band and, in a minor extent, the HF band are modified by the sympathetic system during stressful conditions. Whereas the parasympathetic system affects only to the HF band [1].

The first peak of the LF band is at about 0.1 Hz. Although the origin of this peak is uncertain, it can be explained by baroreflex regulation, which creates the so-called Mayer waves in the blood pressure signal [4]. On the other hand, respiratory sinus arrhythmia (RSA) is a rhythmical fluctuation in the RR-tachogram due to parasympathetic activity, which is synchronized with the respiratory cycle. Such oscillation manifests itself as a peak in the HF band at 0.25 Hz [5].

A mathematical model for the generation of ECG signals with appropriate HRV spectra has been the subject of many research efforts. One of the pioneering studies was developed by McSharry *et al.* [2]. They proposed a method to produce tachogram signals with specific statistics of the HR and frequency-domain characteristics of HRV. Other models that include the effects of sympathetic and parasympathetic system in the heart rate, using a statistical approach similar to the used in Ref. [2] have also been proposed [6]–[10]. They are based on modification to the Zeeman model [11]. For example, Jafarnia-Dabanloo *et al.* [6] developed a model based on a modified Zeeman model to produce the RR-tachogram, which uses a simple neural network to generate an ECG cycle.

An ECG signal obtained from a single lead offers useful information. Part of this information can be extracted from the vector electrocardiogram, which is grounded on the assumption that the human body is a volume conductor. The so-called *lead vector*, is the spatial vector associated to an electrode pair, located at certain position on the surface of

MAQJ (CVU-446274) acknowledges postdoctoral financial support from the CONACyT through grant ICN-UNAM-284372. RVM and OJR thank financial support from IPN-México, through grant SIP-IPN-20181398 and SIP-IPN-20182124, respectively. MAQJ, RVM and JLA wish to thank DGAPA-UNAM-PAPIIT for financial support through grant IN110817. MR and ER acknowledge the support by JSPS KAKENHI Grant Number 17K00411. *Asterisk indicates corresponding author.*

M. A. Quiroz-Juárez is with the Instituto de Ciencias Nucleares, Universidad Nacional Autónoma de México, Circuito Exterior S/N, Ciudad Universitaria, 04510 Ciudad de México, México.

O. Jiménez-Ramírez is with the Escuela Superior de Ingeniería Mecánica y Eléctrica, Culhuacán. Instituto Politécnico Nacional. Santa Ana 1000, San Francisco Culhuacán, 04430 Ciudad de México, México.

R. Vázquez-Medina is with the Centro de Investigación en Ciencia Aplicada y Tecnología Avanzada, Instituto Politécnico Nacional, Cerro Blanco 141, Colinas del Cimatario, 76090 Querétaro México, México.

E. Ryzhii is with the Department of Anatomy and Histology, Fukushima Medical University, Fukushima 960-1295, Japan and the Complex Systems Modeling Laboratory, University of Aizu, Aizu-Wakamatsu 965-8580, Japan.

M. Ryzhii is with the Complex Systems Modeling Laboratory, University of Aizu, Aizu-Wakamatsu 965-8580, Japan.

J.L. Aragón is with the Centro de Física Aplicada y Tecnología Avanzada, Universidad Nacional Autónoma de México, Boulevard Juriquilla 3001, Juriquilla, 76230 Querétaro México, México (e-mail: jlaragon@unam.mx).

This article has been accepted for publication in a future issue of this journal, but has not been fully edited. Content may change prior to final publication. Citation information: DOI 10.1109/TNB.2018.2870331, IEEE Transactions on NanoBioscience

the skin. Cardiologists have settled on 12 standard leads. Willem Einthoven, Nobel Prize winner in 1924 in physiology and medicine for the invention of the first electrocardiograph, established the first three leads (I, II and III), which are called *bipolar limb leads*. He hypothesized that the lead vectors associated with the readings of I, II and III form an equilateral triangle in the vertical, frontal plane of the body, given by the unit vectors [12, Ch.12]. The *augmented limb leads* (Leads aVR, aVL and aVF) are combination leads of the same three electrodes as I, II and III, but considering Goldberger's central terminal as a negative pole [13], [14]. Finally, *precordial leads* are unipolar potentials referenced to a common electrode known as the Wilson central terminal (Leads $V1$-$V6$) [15], [16].

Some discrepancies in the measurements can occur because the lead vectors are not known with enough accuracy. However, for clinical purposes, the information gleaned from this simple approximation is remarkably useful.

Given the importance of information obtained from ECG recordings for medical education and equipment testing some hardware and software simulators that offer the generation of ECG signals from all 12 leads (or some of them) have been published in the literature [17]–[20]. However, such implementations keep shortcomings in the amplitudes, ranges, waveforms and intervals of the produced signals. Shorthen and Burke [19] reported the design and development of an ECG signal generator using a 16-bit microcontroller of the PIC24 family. The generator reproduce only Lead II signal with physiologically right timing and profile characteristics. Jóśko and Rak [20] proposed the design of a platform for acquisition, processing, presenting, and distributing ECG data. In their system, standard ECG source can be accelerated and moderated in a wide range, and signals with different noise level and power line interference impacts can be produced.

It is important to mention that the ECG source of the artificial simulators are based on sampled waveform previously stored in memory. Therefore, they do not provide a useful tool to a dynamical interpretation of abnormalities in the cardiac conduction system.

In this work, we extend the recent heterogeneous nonlinear oscillator model of cardiac conduction system [21], by including an artificial RR-tachogram with HRV spectrum. The modified model is capable to generate all the standard 12 leads representing human body surface ECG. Additionally, we introduce ambient noise and the respiratory frequency into baseline wander, to reproduce realistic ECG signals. The proposed model provides a useful tool for educational and testing purposes (for example, for heart failure prediction systems such as presented in [22]) and can be considered as an initial step for the development of a 12 lead ECG simulator with a wide range of possibilities, accounting for biophysical properties of the human heart.

II. Methods

A. The Model

We use as a starting point the model of cardiac conduction system [21] consisting of sets of heterogeneous nonlinear oscillators, which represent electrical responses of main natural pacemakers and atrial (AT) and ventricular (VN) muscles. Recently, the model was applied to simulate the appearance of ventricular fibrillation as an instance of chaos by inclusion of an ectopic pacemaker [23].

Sinoatrial (SA) node, atrioventricular (AV) node and His-Purkinje (HP) system are represented by modified Van der Pol-type (VdP) oscillators [24]–[27] connected with time-delay velocity coupling, given by the following sets of ordinary differential equations, where x_i represent action potentials of natural pacemakers:

$$\begin{aligned} \tfrac{dx_i}{dt} &= y_i, \\ \tfrac{dy_i}{dt} &= -F(x_i)y_i - G(x_i) + K_{\text{node}}\left(y_{i-1}^{\tau_{\text{node}}} - y_i\right). \end{aligned} \tag{1}$$

Here, $F(x_i) = a_i\left(x_i^2 - u\right)$ are the damping terms and $G(x_i) = f_i x_i(x_i + d)(x_i + e_i)$ are the harmonic force terms, the index $i = 1, 2, 3$ corresponds to SA, AV and HP nodes, respectively, K_{node} denotes the particular coupling constant for each pacemaker ($K_{\text{AV-SA}}$, $K_{\text{SA-AV}}$ and $K_{\text{AV-HP}}$), $y_i^{\tau_{\text{node}}} = y_i(t - \tau_{\text{node}})$ are the time-delayed coupling components, and τ_{node} is corresponding coupling time delay [21]. The terms a_i, f_i, u, d and e_i are the parameters of each oscillator. The coupling constant $K_{\text{AV-SA}}$ is set to zero since only unidirectional coupling between the pacemakers is considered. Thus for $i = 1$, the corresponding component of the coupling current vanishes.

The description of the electrical responses of AT and VN muscles under the stimulation by the pacemakers is based on modified FitzHugh-Nagumo oscillators [28]–[30], as described in Ref. [21]:

$$\begin{aligned} \tfrac{dz_j}{dt} &= k_j\left(-c_j z_j\left(z_j - w_{j1}\right)\left(z_j - w_{j2}\right) - b_j v_j - g_j v_j z_j + I_j\right), \\ \tfrac{dv_j}{dt} &= k_j h_j\left(z_j - v_j\right), \end{aligned} \tag{2}$$

where $j = 1, \ldots, 4$ refers to the P-wave, Ta-wave, QRS complex and T-wave, respectively; $I_j = C_j Y_j H(Y_j)$ is the magnitude of the stimulation current that couples the SA and HP pacemaker to AT and VN muscles, respectively, C_j are the corresponding coupling coefficients, $H(Y)$ is the Heaviside step function, $Y_1 = y_1$, $Y_2 = -y_1$, $Y_3 = y_3$, $Y_4 = -y_3$ from (1); the parameters k_j, c_j, w_{j1}, w_{j2}, b_j, h_j and g_j control the rest state, the excitability, the duration of the action potential, the excitation threshold and excited state of each oscillator.

The net ECG waveform is calculated as a composition of muscle electrical responses in the following way,

$$ECG = z_0 + z_1 - z_2 + z_3 + z_4, \tag{3}$$

where z_0 is the baseline value of the ECG signal.

The purpose of this work was to develop relatively simple heart model that includes an artificial RR-tachogram, additive noise, a baseline wander coupled with the respiratory frequency, and the ability to generate signals of all 12 standard ECG leads. The conceptual framework of the extended model is presented in Fig. 1.

This article has been accepted for publication in a future issue of this journal, but has not been fully edited. Content may change prior to final publication. Citation information: DOI 10.1109/TNB.2018.2870331, IEEE Transactions on NanoBioscience

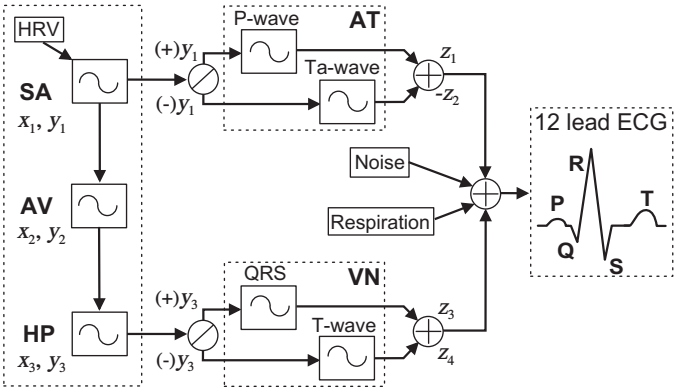

Fig. 1. General scheme of the proposed model.

B. Heart Rate Variability

The development of a dynamical model for the generation of ECG signals with appropriate HRV spectra is a subject that has been widely investigated. McSharry *et al.* [2] proposed a method to produce tachogram signals with specific statistics such as the mean and standard deviation of the HR and frequency-domain characteristics of HRV. Such features were incorporated in a dynamical model of three coupled ordinary differential equations, capable to generate realistic synthetic ECG signals. They incorporated the effect of both RSA and Mayer waves in the power spectrum $S(f)$ by generating RR-intervals having a bimodal power spectrum consisting of the sum of two Gaussian distributions,

$$S(f) = \sum_{i=1}^{2} \frac{\sigma_i^2}{\sqrt{2\pi\gamma_i^2}} e^{-\frac{(f-f_{ri})^2}{2\gamma_i^2}}, \tag{4}$$

with means f_{r1}, f_{r2} and standard deviations γ_1, γ_2, respectively; power in the LF and HF bands are given by σ_1^2 and σ_2^2, respectively, whereas the variance equals the total area $\sigma^2 = \sigma_1^2 + \sigma_2^2$, yielding an LF/HF ratio of σ_1^2/σ_2^2.

A RR-interval time series $T(t)$ with power spectrum $S(f)$ is generated by

$$T(t) = F^{-1}\left\{CS(f)\right\}, \tag{5}$$

where F^{-1} is the inverse Fourier transform and $CS(f)$ is a sequence of complex numbers with amplitudes $\sqrt{S(f)}$ and randomly distributed phases between 0 and 2π.

Notice that (5) allows to produce a time series with any desired mean and standard deviation if the right hand side is multiplied by an appropriate scaling factor and an offset value is included. In [2], the authors incorporate the RR-tachogram $T(t)$ into the angular frequency ω of the limit cycle generated by their dynamical model (as $\omega(t) = 2\pi/T(t)$), because the time required to complete one lap of the limit cycle is equal to the RR-interval of the ECG signal.

C. Fitting of Model Parameters to Real ECG Signal

Many various models utilizing different approaches to fit model parameters and to reconstruct real ECG records were published previously (see, for example, [31]–[33]). With the model presented here, we can synthesize the ECG waveform for each of 12 standard leads for normal and pathological cases, as well as fit it to individual characteristics of a subject considering weighted linear combination of the solution of the system (2), that is, a weighted sum of the depolarization and repolarization responses:

$$ECG = z_0 + \alpha_1 z_1 - \alpha_2 z_2 + \alpha_3 z_3 + \alpha_4 z_4. \tag{6}$$

The weighting coefficients $\alpha_1, \ldots, \alpha_4$ for each lead are obtained by a fitting procedure with real ECG's. For this purpose, we import the ideas of a supervised learning algorithm called perceptron [34], [35], which is recognized as the simplest type of artificial neural network. In our particular case, before starting the optimization process, the perceptron is subjected to a learning stage that consists of adjusting the weights of each input, based on the difference between the obtained input and the desired output. Novikoff [36], [37] shown that this learning algorithm converges after a finite number of iterations.

To implement a fitting procedure, we first define:

- $ECG_r(t_i)$ is the desired signal (real ECG) at times $t_1, t_2, \ldots, t_N$.
- $ECG_e(t_i)$ is the estimated ECG signal evaluated at times $t_1, t_2, \ldots, t_N$..
- $\{z_1(t), z_2(t), z_3(t), z_4(t)\}$ are the input signals (responses of the modified FitzHugh-Nagumo model).
- $\{\alpha_1(n), \alpha_2(n), \alpha_3(n), \alpha_4(n)\}$ are the weights at the n-th iteration.
- γ is the convergence rate, and
- ϵ is a specified threshold error.

Since the perceptron is a linear binary classificator (that is, considers binary inputs) some modifications should be applied to the original algorithm since our input data are signals. We then implement the following algorithm:

1) Initialize the set $\{\alpha_1(0), \ldots, \alpha_4(0)\}$ to random values.
2) Solve system (2) to get the ECG_e as (6):

$$ECG_e(t_i) = \sum_{i=1}^{4} \alpha_i(n) z_i(t_i).$$

notice that z_0 is not considered since it only represents a baseline.

3) With the real data, the estimated error is

$$e(t_i) = ECG_r(t_i) - ECG_e(t_i)$$

4) Update the weights $\alpha_i(n)$ as

$$\alpha_i(n+1) = \alpha_i(n) + \gamma \int_a^b e(t_i) z_i(t_i),$$

where a discrete integration method (such as trapezoid) should be used.

Steps 2, 3 and 4 are repeated until the error integral is less than ϵ, that is

$$\int_a^b e(t) z_i(t) \leq \epsilon.$$

The data points from the real ECG's at times $t_1, t_2, \ldots, t_N$ were obtained by digitizing the signal using the free software *Enguage Digitizer* [38].

This article has been accepted for publication in a future issue of this journal, but has not been fully edited. Content may change prior to final publication. Citation information: DOI 10.1109/TNB.2018.2870331, IEEE Transactions on NanoBioscience

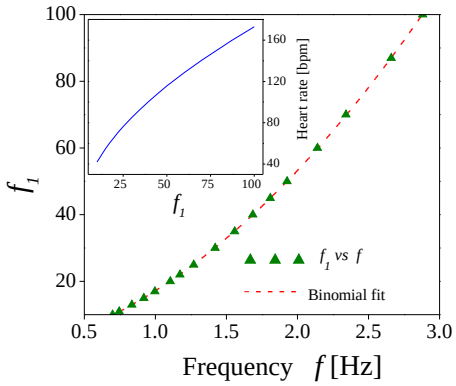

Fig. 2. Dependence of the parameter f_1 on the frequency (green triangles) and its binomial fitting function (dashed red line) of this curve given by (7). Inset shows heart rate as a function of the parameter f_1 [21].

III. Results

A. Realistic ECG Signal

The intrinsic frequencies of the natural pacemakers are controlled by the parameters f_i. To maintain stable synchronization between the oscillators while the SA rate changes, the coupling coefficients were set to be proportional to f_1: $K_{SA-AV} = K_{AV-HP} = f_1$. In the inset of Fig. 2 shows dependence of the heart rate on the parameter f_1. Given this dependence, we propose that the variations of the RR-intervals in a regular sinus rhythm (with specific statistics) can be incorporated through the variation of the parameter f_1. Since in the model the heart rate depends nonlinearly on f_1, we obtained f_1 dependence on mean frequency f and fit it with binomial function (see Fig. 2):

$$\phi = -0.7319 + 8.798f + 9.098f^2, \tag{7}$$

where $f = 1/T_d(t)$, and $T_d(t)$ is a scaled time series with the offset $T_d(t) = \alpha + \beta T(t)$. The scaling factor β and offset α can be calculated from a specified mean HR_{mean} and standard deviation HR_{std} of heart rate, as follows:

$$\alpha = \frac{60}{HR_{mean}}, \quad \beta = \left(\frac{\alpha}{\sigma_T}\right)\left(\frac{HR_{std}}{HR_{mean}}\right), \tag{8}$$

where σ_T is the standard deviation of $T(t)$. In this way, the heart rate variability can be incorporated into the 2R model as follows:

1) Apply (5) to produce the synthetic RR-tachogram with HRV spectrum,
2) Scale the time series $T(t)$ and include an offset value to get a desired mean and standard deviation (8),
3) Set f_1 as a function of $T_d(t)$, as in (7).

With this, f_1 will change dynamically and variations in the length of RR-intervals can be expected.

Additionally, a new baseline wander can be introduced by coupling the respiratory frequency f_0 with the baseline value z_0 in (3) as follows:

$$z_n(t) = z_0 \, sin(2\pi f_0 t). \tag{9}$$

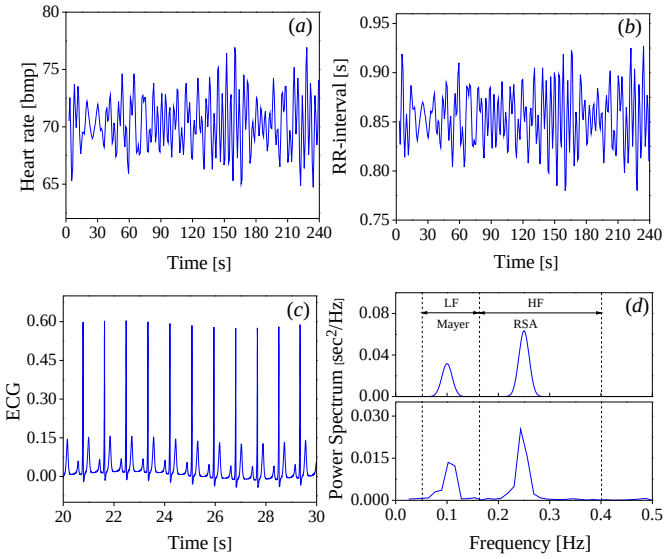

Fig. 3. Analysis of RR-intervals from R-peak detection of the ECG signal generated using the proposed method. (a) Variation of instantaneous heart rate, (b) RR-intervals, (c) calculated ECG signal, and (d) power spectra of the RR-intervals: top - obtained with (4) and bottom - from the calculated ECG.

Numerical simulations of the presented model were carried out with the following parameter values for a normal rhythm. For the natural pacemakers: $a_1 = 40$, $a_2 = a_3 = 50$, $u = 0.69$, $f_1 = 22$, $f_2 = 8.4$, $f_3 = 1.5$, $d = 3$, $e_1 = 3.5$, $e_2 = 5$ and $e_3 = 12$; for the muscles: $k_1 = 2 \times 10^3$, $k_2 = 1 \times 10^2$, $k_3 = 1 \times 10^4$, $k_4 = 2 \times 10^3$, $c_1 = 0.26$, $c_2 = c_3 = 0.12$, $c_4 = 0.1$, $b_1 = b_2 = b_4 = 0$, $b_3 = 0.015$, $g_1 = 0.4$, $g_2 = g_3 = 0.09$, $g_4 = 0.1$, $h_1 = 0.004$, $h_2 = h_3 = h_4 = 0.008$, $w_{11} = 0.13$, $w_{12} = 1.0$, $w_{21} = w_{31} = 0.12$, $w_{22} = w_{32} = 1.1$, $w_{41} = 0.22$, $w_{42} = 0.8$, $C_1 = 4 \times 10^{-5}$, $C_2 = -4 \times 10^{-5}$, $C_3 = 9 \times 10^{-5}$ and $C_4 = -6 \times 10^{-5}$. For the baseline wander the parameter values are $z_0 = 15$ mV and $f_0 = 0.1$ Hz.

In Figs. $3(a)$ and $3(b)$, instantaneous heart rate in beat-per-minute (bpm) and RR-intervals are shown, respectively; the mean rate of 70 bpm and standard deviation of 5 bpm were considered. Resulting realistic ECG signal generated using the presented method with the RR-intervals modulated by the incorporated HRV and the base wander is shown in Fig. 3(c). In order to confirm the effect of both RSA and Mayer waves on the calculated RR-tachogram, we obtained power spectrum and compared it with the spectrum of function $S(f)$ (4). Figure $3(d)$ demonstrates the power spectrum (4) (top) considering the parameters: $f_{r1} = 0.1$, $f_{r2} = 0.25$, $\gamma_1 = 0.01$, $\gamma_2 = 0.01$ and $\sigma_1^2/\sigma_2^2 = 0.5$, and the spectrum from the calculated ECG (bottom). Two active frequencies at 0.1 Hz (Mayer wave) and 0.25 Hz (RSA wave) can be discerned.

The QT-interval is the elapsed time between the beginning of the QRS complex and the end of the T-wave, and represents the electrical depolarization and repolarization of the ventricles. Both the RR and the QT intervals depend on the heart rate, and they are used in clinical practice to analyze real ECGs. Figure $4(a)$ shows the RR and QT intervals dependence on the parameter f_1, calculated with the proposed model. We

This article has been accepted for publication in a future issue of this journal, but has not been fully edited. Content may change prior to final publication. Citation information: DOI 10.1109/TNB.2018.2870331, IEEE Transactions on NanoBioscience

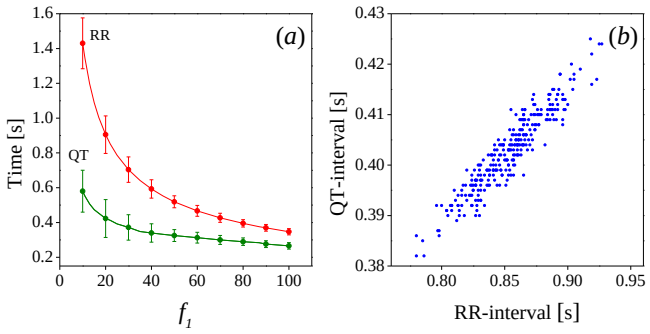

Fig. 4. RR and QT intervals of ECG calculated with the proposed model. (a) Dependences of RR (red line) and QT (green line) intervals on the parameter f_1. The red and green dots represent the mean RR and QT intervals, respectively, for ten values of the parameter f_1, and error bars correspond to the standard deviation of the tachograms generated for each parameter value. (b) Relationship between RR and QT intervals.

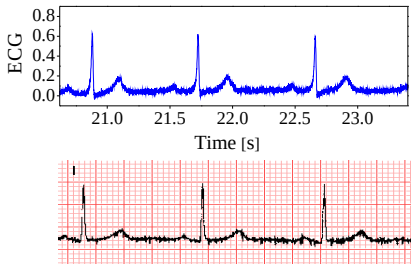

Fig. 5. Comparison between obtained ECG generated by the presented model with normally distributed additive noise (top panel) and real ECG signal from a normal human (bottom panel, taken from Ref. [43]).

obtained $f_1(t)$ and $T_d(t)$ series for ten fixed values of the parameter f_1: in the range 10...100; a standard deviation of 3 bpm was considered for all simulations. In Fig. $4(a)$, the mean RR and QT intervals are denoted as red and green dots, respectively, and the standard deviations of the tachograms are shown by error bars.

Abnormalities of QT-intervals can unveil potential ventricular arrhythmias and the risk of a sudden cardiac death. To create a comparison of the QT-interval with reference values, a correction formula for the heart rate should be applied [39], which linearly relates the QT and RR intervals [40]–[42]. Figure $4(b)$ demonstrates similar a linear relationship between the RR and QT intervals, which makes evident the capacity of our model to reproduce realistic ECG characteristics, providing a suitable tool to study QT dispersion as function of the RR-interval variability.

Also, the observational uncertainty is incorporated by including normally distributed additive noise with zero mean and 7.0 mV standard deviation. A qualitative comparison of a real ECG signal (standard Einthoven lead I [43]) with our results is shown in Fig. 5.

B. 12 Lead ECG Signal

As it was mentioned in Section I, each one of the 12 ECG leads records the electrical activity of the heart from a different angle [44], representing the projection of the dipole along the line defined by the leads. From the combination of these electric cardiac events, the standard ECG waveform of each lead can be obtained. Of course, some of these signals may be preponderant in this composition, according to the variable angle that is observed.

In the proposed model, the synthetic ECG signal is a combination of the atrial and ventricular muscle electrical signals, where the depolarization and repolarization waves are described as separate processes based on modified FitzHugh-Nagumo systems (3). Under this assumption, it is possible to establish the shape of each lead by means of a weighted sum of the depolarization and repolarization responses. Thus, to obtain the 12 lead ECG waveforms we use the following weighted linear combination (6).

The weighting coefficients $\alpha_1, \ldots, \alpha_4$ for each lead were obtained with a modification of the *perceptron* algorithm, as described in Section II-B and are specified in Table I. The initial conditions are: $x_i = -0.1$, $y_i = 0.025$, $z_i = 0.0$ $v_i = 0$, for $i = 1, \ldots, 4$. The number of iterations for the fitting algorithm required to obtain specific precision is also indicated in the rightmost column of the Table I and subsequent tables.

Figure 6 shows the 12 lead ECG signals with realistic heart rate dynamic generated by the presented model (1)-(2) and

TABLE I
WEIGHTING COEFFICIENTS FOR THE NORMAL 12 LEAD ECG SIGNALS

Lead	Parameter Values				Iterations
	α_1	α_2	α_3	α_4	
I	0.5616	-0.03012	0.4969	0.3964	212
II	1.6768	-0.0602	0.9941	1.199	249
III	1.1243	-0.03005	0.497	0.801	241
aVR	-0.6483	0.0367	-0.5964	-0.7009	255
aVL	0.8046	-0.0133	0.1985	-0.397	140
aVF	0.64455	-0.0478	0.7949	0.7008	207
V1	0.4565	0.3979	-0.3981	0.2983	185
V2	0.1119	1.288	-1.2508	2.9995	199
V3	1.3145	1.2969	-0.3854	1.803	210
V4	1.709	1.2996	-0.1962	1.2001	268
V5	1.5093	1.1981	-0.0863	0.9036	240
V6	0.7485	-0.0367	0.7972	0.40003	84

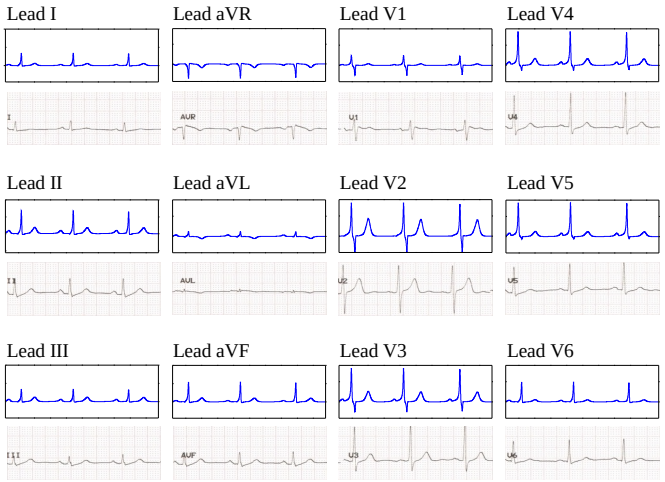

Fig. 6. Calculated 12 lead ECG signals with specific statics in the heart rate, obtained with the proposed model (top panels). For comparison, real ECG signals (taken from Ref. [45]) are also shown (bottom panels).

This article has been accepted for publication in a future issue of this journal, but has not been fully edited. Content may change prior to final publication. Citation information: DOI 10.1109/TNB.2018.2870331, IEEE Transactions on NanoBioscience

TABLE II
WEIGHTING COEFFICIENTS FOR THE WELLENS SYNDROME

Lead	Parameter Values				Iterations
	α_1	α_2	α_3	α_4	
V1	-0.3298	-0.3244	-0.1001	-0.4506	232
V2	0.1597	0.1773	-0.77	-0.8913	236
V3	0.2503	0.2594	-1.1644	-1.5269	211

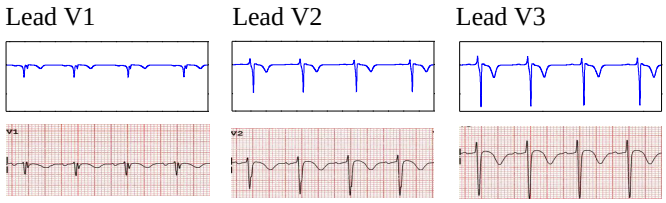

Fig. 7. V1-V3 precordial leads ECG signals of Wellens syndrome, Type 1, ischemia obtained with the proposed model (top panels) calculated with the weighting parameters given in Table II. For comparison, real ECG signals (taken from Ref. [45]) are also shown (bottom panels).

(4)-(6). Additionally, comparisons with real ECG signals [45] are presented. We observe a qualitative agreement, that is, our model is able to capture the general behavior of the real ECGs. Also, notice that the α_i coefficients for the bipolar limb leads satisfy the Einthoven triangle.

To illustrate the importance of generating 12 lead ECG records identifying potential abnormalities in the heart, we considered the Wellens syndrome, Type 1, ischemia, which is an ECG abnormality associated with significant left anterior descending coronary artery stenosis. Elevation of the ST segment and inversion of the T-wave are characteristic patterns of the syndrome, which are maximal and clearly identifiable in leads V1, V2, and V3, and ECG signals in the rest of the leads are normal. A quick identification of the ST-T abnormalities is of great importance to detect life-threatening disorders, such as myocardial infarction [46]. In Fig. 7, the simulation results for precordial leads V1, V2, and V3 for the Wellens syndrome, Type 1, ischemia are shown and compared with real ECG records [45].

Notice that ST-segment elevation and T-wave inversion demonstrated on the obtained ECG are very similar to the real ones. The weighting coefficients $\alpha_1, ..., \alpha_4$ for this case are given in Table II.

C. Fitting of ECG Waveforms to Particular Subjects' Data

The perceptron algorithm was used to fit calculated to real ECG of particular subjects. In particular, we calculated the weighting parameters and obtained all the 12 ECG leads signals for nornal sinus rhythm of thirteen subjects, with data taken from PhysioNet database [47]. The data sets for the fitting correspond to nine men and four women subjects aged 26 to 69.

The mean absolute error

$$F = \frac{1}{M}\int_0^T \left| ECG_r(t_i) - ECG_e(t_i) \right|, \qquad (10)$$

was used to quantify the absolute deviation between the real and fitted ECGs. Here, $ECG_r(t_i)$ and $ECG_e(t_i)$ are the real and estimated ECG signals, respectively, at times $t_1, t_2, ..., t_M$ and T is the period. Equation (10) was normalized with respect to the number of samples M and the integration has been implemented numerically with the trapezoid method. It should be mentioned that this criterion, as well as slight modifications of it, has been employed in several other works as indicator of convergence for the parameter identification methods [31], [48]–[50].

In order to show the invariance of the error with respect to the number of subjects, the cumulative average of Equation (10) for each lead was calculated as,

$$e_r = \frac{1}{N}\sum_{i=1}^{N} F_N, \qquad (11)$$

where N denotes the number of subjects.

In Fig. 8 e_r as function of N for full 12-lead ECG datasets is shown. We observe an asymptotic convergence of the error for all the leads. Note that, the consideration of thirteen subjects was sufficient to observe an invariance condition of the error.

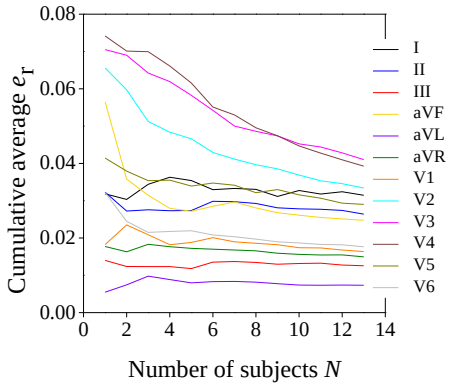

Fig. 8. Calculated cumulative average e_r of each lead versus number of subjects N.

Additionally, from the estimated ECG signals, we obtained the mean ECG signal and its standard deviation for each lead. In Fig. 9, the solid line represents the mean ECG signal and the shaded region corresponds to the standard deviation. Figure 9 demonstrates relatively good matching of the shapes and amplitudes of the calculated and real ECG waveforms.

Finally, in Table III the average weighting parameters for each lead obtained from the estimated ECG signals of the thirteen subjects are shown.

IV. CONCLUSION

We proposed an extension of a previously developed heterogeneous oscillator model of cardiac conduction system [21], with the aim to generate the 12 lead ECG signals with appropriate heart rate variability spectra. The upgraded model incorporates an artificial RR-tachogram with specific statistic on the heart rate, in particular, both respiratory sinus arrhythmia and Mayer waves are introduced in the HRV spectrum. Additive ambient noise and a baseline wander are also added to account for observational uncertainty of real ECG signals. The proposed model reproduces QT and RR

This article has been accepted for publication in a future issue of this journal, but has not been fully edited. Content may change prior to final publication. Citation information: DOI 10.1109/TNB.2018.2870331, IEEE Transactions on NanoBioscience

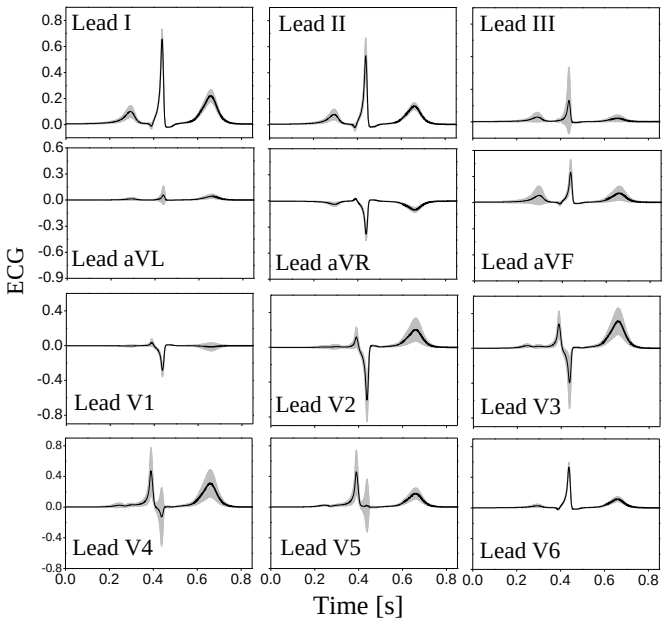

Fig. 9. Mean ECG signals (solid line) and their standard deviations (shaded region) for each of the 12 leads calculated from estimated ECG of thirteen particular subjects as described in the text.

TABLE III
AVERAGE WEIGHTING COEFFICIENTS FOR THE NORMAL 12 LEAD ECG SIGNALS

Lead	Average Parameter Values			
	$\overline{\alpha_1}$	$\overline{\alpha_2}$	$\overline{\alpha_3}$	$\overline{\alpha_4}$
I	1.9566	-0.0667	1.0781	1.5638
II	1.5469	-0.0696	0.8705	1.0186
III	0.5682	0.0029	0.2037	0.1532
aVR	-0.7509	0.0678	-0.6281	-0.7289
aVL	0.2731	-0.0037	0.1026	0.3077
aVF	1.6385	-0.0474	0.5982	0.7631
V1	-0.0642	0.0742	-0.4678	-0.1019
V2	0.2769	0.2411	-1.0371	1.4462
V3	0.9089	0.5191	-0.7036	2.1496
V4	0.6677	0.7796	-0.2363	2.2085
V5	0.5761	0.7216	0.00766	1.2517
V6	0.531	-0.0679	0.8745	0.8225

intervals variations similar to clinically observed ECGs. We also obtained full 12 lead ECG waveforms from a weighted linear combination of atrial and ventricular muscle signals. We demonstrated that the model is capable to simulate accurately realistic ECG characteristics, even local pathological phenomena, such as, the Wellens syndrome, Type 1, ischemia. Moreover, we have shown in our preliminary calculations that it is possible to develop personalized cardiac conduction model using proposed fitting method.

The proposed model can serve as a useful tool for medical education and testing, such as software and hardware ECG signal processing systems,including, with further extension to simulation intracardiac signals, testbeds for implantable cardiac devices.

REFERENCES

[1] T. force of the European Society of Cardiology, the North American Society of Pacing, and Electrophysiology, "Heart rate variability. standards of measurement, physiological interpretation, and clinical use. task force of the european society of cardiology and the north american society of pacing and electrophysiology," *Circulation*, vol. 93, pp. 1043–1065, 1996.

[2] P. E. McSharry, G. D. Clifford, L. Tarassenko, and L. A. Smith, "A dynamical model for generating synthetic electrocardiogram signals," *IEEE Trans. Biomed. Eng.*, vol. 50, no. 3, pp. 289–294, 2003.

[3] A. H. Khandoker, C. Karmakar, M. Brennan, M. Palaniswami, and A. Voss, *Poincaré plot methods for heart rate variability analysis*. Springer, 2013.

[4] R. de Boer, J. Karemaker, and J. Strackee, "Hemodynamic fluctuations and baroreflex sensitivity in humans: a beat-to-beat model," *Am. J. Physiol.*, vol. 253, no. 3, pp. H680–H689, 1987.

[5] G. G. Berntson, J. T. Cacioppo, and K. S. Quigley, "Respiratory sinus arrhythmia: Autonomic origins, physiological mechanisms, and psychophysiological implications," *Psychophysiology*, vol. 30, no. 2, pp. 183–196, 1993.

[6] N. Jafarnia-Dabanloo, D. C. McLernon, H. Zhang, A. Ayatollahi, and V. Johari-Majd, "A modified Zeeman model for producing HRV signals and its application to ECG signal generation," *J. Theor. Biol.*, vol. 244, no. 2, pp. 180–189, 2007.

[7] D. C. Mclernon, N. J. Dabanloo, A. Ayatollahi, V. J. Majd, and H. Zhang, "A new nonlinear model for generating RR tachograms," *Comput. Cardiol.*, vol. 31, pp. 481–484, 2004.

[8] S. L. M. Abad, N. J. Dabanloo, and M. Mohagheghi, "Different approaches for linear and non-linear ECG generation," in *Proc. 1st Int. Conf. Biomed. Eng. Informatics, BMEI 2008*, vol. 2, 2008, pp. 415–419.

[9] S. L. M. Abad, N. J. Dabanloo, S. B. Jameie, and K. Sadeghniiat, "A developed Zeeman model for HRV signal generation in different stages of sleep," in *Proc. 13th Int. Conf. Biomed. Eng.*, Springer, 2009, pp. 219–222.

[10] A. Ayatollahi, N. J. Dabanloo, D. McLernon, V. J. Majd, and H. Zhang, "A comprehensive model using modified Zeeman model for generating ECG signals," *Iranian J. Electrical Electronic Eng.*, vol. 1, no. 2, pp. 88–93, 2005.

[11] E. C. Zeeman, *Differential equations for the heartbeat and nerve impulse*. Mathematics Institute, University of Warwick, 1972.

[12] J. P. Keener and J. Sneyd, *Mathematical Physiology. II: Systems Physiology.* Springer, 2008.

[13] E. Goldberger, "A simple, indifferent, electrocardiographic electrode of zero potential and a technique of obtaining augmented, unipolar, extremity leads," *Am. Heart J.*, vol. 23, pp. 483–492, 1942.

[14] ——, "The aVl, aVr, and aVf leads," *Am. Heart J.*, vol. 24, no. 3, pp. 378–396, 1942.

[15] F. N. Wilson, A. G. Macleod, and P. S. Barker, "The potential variations produced by the heart beat at the apices of einthoven's triangle," *Am. Heart J.*, vol. 7, no. 2, pp. 207–211, 1931.

[16] F. N. Wilson, F. D. Johnston, A. Macleod, and P. S. Barker, "Electrocardiograms that represent the potential variations of a single electrode," *Am. Heart J.*, vol. 9, pp. 447–458, 1934.

[17] C. Caner, M. Engin, and E. Z. Engin, "The programmable ECG simulator," *J. Med. Syst.*, vol. 32, no. 4, pp. 355–359, 2008.

[18] M. J. Burke and M. Nasor, "An accurate programmable ECG simulator," *J. Med. Eng. Technol.*, vol. 25, no. 3, pp. 97–102, 2001.

[19] G. P. Shorten and M. J. Burke, "A precision ECG signal generator providing full Lead II QRS amplitude variability and an accurate timing profile," in *Proc. 31st Annual Int. Conf. of the IEEE Eng. Med. Biol. Soc.: Engineering the Future of Biomedicine, EMBC 2009*, 2009, pp. 3008–3011.

[20] A. Jóśko and R. J. Rak, "Effective simulation of signals for testing ECG analyzer," *IEEE Trans. Instrum. Meas.*, vol. 54, no. 3, pp. 1019–1024, 2005.

[21] E. Ryzhii and M. Ryzhii, "A heterogeneous coupled oscillator model for simulation of ECG signals," *Comput. Methods Programs Biomed.*, vol. 117, no. 1, pp. 40–49, 2014.

[22] A. Mdhaffar, I. B. Rodriguez, K. Charfi, L. Abid, and B. Freisleben, "CEP4HFP: Complex event processing for heart failure prediction," *IEEE Trans. Nanobiosci.*, vol. 16, no. 8, pp. 708–717, 2017.

[23] M. A. Quiroz-Juárez, R. Vázquez-Medina, E. Ryzhii, M. Ryzhii, and J. L. Aragón, "Quasiperiodicity route to chaos in cardiac conduction model," *Commun. Nonlinear Sci. Numer. Simul.*, vol. 42, pp. 370–378, 2017.

[24] D. Postnov, S. K. Han, and H. Kook, "Synchronization of diffusively coupled oscillators near the homoclinic bifurcation," *Phys. Rev. E*, vol. 60, no. 3, pp. 2799–807, 1999.

[25] S. R. Gois and M. a. Savi, "An analysis of heart rhythm dynamics using a three-coupled oscillator model," *Chaos Soliton. Fract.*, vol. 41, no. 5, pp. 2553–2565, 2009.

[26] K. Grudziński and J. J. Zebrowski, "Modeling cardiac pacemakers with relaxation oscillators," *Physica A*, vol. 336, no. 1–2, 2004, pp. 153–162.

[27] J. Żebrowski, K. Grudziński, T. Buchner, P. Kuklik, J. Gac, G. Gielerak, P. Sanders, and R. Baranowski, "Nonlinear oscillator model reproducing various phenomena in the dynamics of the conduction system of the heart," *Chaos*, vol. 17, no. 1, p. 015121, 2007.

[28] R. FitzHugh, "Impulses and physiological states in theoretical models of nerve membrane," *Biophysical J.*, vol. 1, no. 6, pp. 445–466, 1961.

[29] J. Nagumo, S. Arimoto, and S. Yoshizawa, "An active pulse transmission line simulating nerve axon," *Proc. the IRE*, vol. 50, no. 10, pp. 2061–2070, 1962.

[30] J. M. Rogers and A. D. McCulloch, "A collocation-galerkin finite element model of cardiac action potential propagation," *IEEE Trans. Biomed. Eng.*, vol. 41, no. 8, pp. 743–757, 1994.

[31] S. Das and K. Maharatna, "Fractional dynamical model for the generation of ECG like signals from filtered coupled Van-der Pol oscillators," *Comput. Methods Programs Biomed.*, vol. 112, pp. 490–507, 2013.

[32] R. Sameni, G. D. Clifford, C. Jutten, and M. B. Shamsollahi, "Multichannel ECG and noise modeling: Application to maternal and fetal ECG signals," *EURASIP J. Adv. Signal Process.*, vol. 2007, pp. 43407–1–14, 2007.

[33] H. Baali, R. Akmeliawati, M. J. E. Salami, A. Khorshidtalab, and E. Lim, "ECG parametric modeling based on signal dependent orthogonal transform," *IEEE Signal Process. Lett.*, vol. 21, no. 10, pp. 1293–1297, 2014.

[34] F. Rosenblatt, "The perceptron: A probabilistic model for information storage and organization in the brain," *Psychol. Rev.*, vol. 65, no. 6, pp. 386–408, 1958.

[35] F. Rosenblatt, "The perceptron – a perceiving and recognizing automaton," Cornell Aeronautical Laboratory, Inc., Buffalo NY, *Tech. Rep. 85-460-1*, 1957.

[36] A. B. Novikoff, "On convergence proofs for perceptrons," Stanford Research Inst., Menlo Park Calif., Tech. Rep., 1963.

[37] M. Minsky, S. A. Papert, and L. Bottou, *Perceptrons: An introduction to computational geometry*. MIT press, 2017.

[38] M. Mitchell, B. Muftakhidinov, T. Winchen, and *et al.* (2017, Nov.) Engauge digitizer software. [Online]. Available: http://markummitchell.github.io/engauge-digitizer

[39] P. Postema and A. Wilde, "The Measurement of the QT Interval," *Curr. Cardiol. Rev.*, vol. 10, no. 3, pp. 287–294, 2014.

[40] I. Schlamowitz, "An analysis of the time relationships within the cardiac cycle in electrocardiograms of normal men: I. the duration of the Q-T interval and its relationship to the cycle length (RR interval)," *Am. Heart J.*, vol. 31, no. 3, pp. 329–342, 1946.

[41] P. Davey, "A new physiological method for heart rate correction of the QT interval," *Heart*, vol. 82, no. 2, pp. 183–186, 1999.

[42] D. Wang, Y. B. Cheung, R. Arezina, J. Taubel, and A. J. Camm, "A nonparametric approach to QT interval correction for heart rate," *J. Biopharm. Stat.*, vol. 20, no. 3, pp. 508–522, 2010.

[43] D. Jenkins and S. Gerred. (2014, Oct.) Ecg library. [Online]. Available: http://www.ecglibrary.com.

[44] V. Fuster, R. A. Walsh, and R. A. Harrington, *Hurst's the Heart*. McGraw-Hill Medical, 2013.

[45] E. Burns. (2017, Mar.) Ecg library. [Online]. Available: http://lifeinthefastlane.com/ecg-library.

[46] E. B. Hanna and D. L. Glancy, "ST-segment depression and T-wave inversion: Classification, differential diagnosis, and caveats," *Cleve. Clin. J. Med.*, pp. 404–414, 2011.

[47] A. L. Goldberger, L. A. N. Amaral, L. Glass, J. M. Hausdorff, P. Ch. Ivanov, R. G. Mark, J. E. Mietus, G. B. Moody, C. K. Peng, and H. E. Stanley, "PhysioBank, PhysioToolkit, and PhysioNet: Components of a new research resource for complex physiologic signals," *Circulation*, vol. 101, no. 23, pp. e215–e220, 2000.

[48] L. Yuan, Q. Yang. "Parameter identification of fractional-order chaotic systems without or with noise: reply to comments," *Commun. Nonlinear Sci. Numer. Simul.*, 2018.

[49] W. H. Ho, J. H. Chou, C. Y. Guo. "Parameter identification of chaotic systems using improved differential evolution algorithm," *Nonlinear Dynamics*, vol. 61, no. 1-2, pp. 29–41, 2010.

[50] X. Li, M. Yin. "Parameter estimation for chaotic systems by hybrid differential evolution algorithm and artificial bee colony algorithm," *Nonlinear Dynamics*, vol. 77, no. 1-2, pp. 61–71, 2014.